Change of composition and surface plasmon resonance of Pd/Au core/shell nanoparticles triggered by CO adsorption

Aimeric Ouvrard, Natalia Alyabyeva, Abdoul-Mouize Zakaria, Keke Yuan, Céline Dablemont, Rémi Lazzari, Fabrice Charra, Bernard Bourguignon

Change of composition and surface plasmon resonance of Pd/Au core/shell nanoparticles triggered by CO adsorption

Aimeric Ouvrard[1,*], Natalia Alyabyeva[1], Abdoul-Mouize Zakaria[1], Keke Yuan[1], Céline Dablemont[1], Rémi Lazzari[2], Fabrice Charra[3], Bernard Bourguignon[1]

[1]Institut des Sciences Moléculaires d'Orsay (ISMO), CNRS, Université Paris-Saclay, 91405 Orsay, France
[2]Institut des NanoSciences de Paris (INSP), CNRS / Sorbonne Université, 75252 Paris, France
[3]Service de Physique de l'État Condensé, SPEC, CEA, CNRS, Université Paris-Saclay, CEA/Saclay, F-91191 Gif sur Yvette, France

*e-mail: aimeric.ouvrard@universite-paris-saclay.fr

ABSTRACT

Controlling composition and plasmonic response of bimetallic nanoparticles (NP) is of great relevance to tune their catalytic activity. Herein, we demonstrate reversible composition and plasmonic response transitions from a core/shell to a bimetallic alloyed palladium/gold NP triggered by CO adsorption and sample temperature. The use of self-organized growth on alumina template film allows scrutinizing the impact of core size and shell thickness onto NP geometry and plasmonic response. Topography, molecular adsorption and plasmonic response are addressed by scanning tunneling microscopy, vibrational sum frequency generation (SFG) spectroscopy and surface differential reflectance spectroscopy, respectively. Modeling CO dipolar interaction and optical reflectivity corroborate the experimental findings. We demonstrate that probing CO adsorption sites by SFG is a remarkably sensitive and relevant method to investigate shell composition and follow in real-time Pd atom migration between the core and the shell. Pd-Au alloying is limited to the first 2 monolayers of the shell and no plasmonic response is found, while for thicker shell, a plasmonic response is observed, concomitant with a lower Pd concentration in the shell. Above 10^{-4} mbar, at room temperature, CO adsorption triggers the shell restructuration forming a Pd-Au alloy that weakens the plasmonic response via Pd migration from the core to the shell. NP annealing at 550 K, after pumping CO, leads to the desorption of remaining CO and gives enough mobility for Pd to migrate back inside the core and recover a pure gold shell with its original plasmonic response. This work demonstrates that surface stoichiometry and plasmonic response can be tuned by using CO adsorption and NP annealing.

KEYWORDS: Core/shell nanoparticles • nanoparticle array • CO adsorption • Pd segregation • surface plasmon resonance • SFG • STM • SDRS • dipolar coupling • finite-element-method

INTRODUCTION

Pd/Au core/shell nanoparticles (NP) have appeared to be very promising for heterogeneous catalysis[1-3] and potentially for plasmon assisted photo-catalysis[4-5]. Their chemical, optical, structural or electronic properties can be tuned by adjusting their composition, dimension or by anchoring molecules at the shell

surface. Determining the inner and surface composition as well as molecular adsorption sites and their relative stability following adsorption is of great importance to control NP reactivity. In this context, CO oxidation reaction is a test bed for Pd/Au catalysts. The reactivity depends intimately on the change of electron density by the addition of second type of atom and on surface structure factor due to the composition changing the activation energy and the nature of active sites for adsorption, dissociation or reaction[2,6-12]. Pd dimers and trimers surrounded by Au atoms have shown a stronger reactivity than extended surfaces for CO oxidation by allowing O_2 adsorption and dissociation[2,13], while the distance between Pd atoms has a crucial role for more complex reaction like vinyl acetate synthesis[1]. Not speaking about mass transport between NPs[14-15], many groups have observed that CO adsorption at room temperature and during oxidation reaction induces important structural changes such as Pd diffusion in the Au shell[10,16-21] or the formation of onion-like inner structural phases[22-23]. The underlying mechanism of CO-induced Pd segregation has been scrutinized in the past decade. The strong affinity of CO to Pd, larger than Pd-Au cohesion energy, is commonly admitted to be the driving force that pulls out Pd atoms to surface. The important role of NP surface defects[20] and edge sites in promoting Pd diffusion has been evidenced[18,24]. Temperature plays also a critical role on Pd by inducing a phase separation or an alloy depending on Pd/Au ratio and the presence of adsorbates[25].

The impact of CO adsorption on Pd/Au NPs has been investigated for various types of samples: NPs supported on powders, colloidal NPs stabilized on a substrate or NPs directly grown on different oxides in vacuum. However, inhomogeneities of size and shape and therefore of active sites often preclude a detailed understanding of the adsorption and catalytic processes with averaging global techniques. In this context, the past two decades have seen the surge of new kinds of relevant supports for heterogeneous catalysis such as Al_2O_3 film on $Ni_3Al(111)$[26], for which self-organization provides long-range ordered NPs with high density and narrow-size distribution. The drastic reduction of inhomogeneous broadening allows probing subtle size and composition effects in NP containing from several atoms[27-30] up to coalescence and with different and controlled core/shell structure[31-32].

Regarding surface composition of core/shell NPs, it is usually investigated by a combination of microscopy, X-ray photoelectron spectroscopy and vibrational spectroscopy. Microscopy techniques can easily reveal effects of CO adsorption on NP shape, but cannot give access directly neither to the chemical composition of the surface nor to the inner particle structure. Photoelectron spectroscopy can reveal depth profile of each element[8-9,19,33-34]. However it requires dedicated setups[35] like environmental electron transmission microscopy[8,10,33] to go beyond the Knudsen regime of pressure at the opposite light-base measurements such as UV/Vis (electronic properties)[11,36] or vibrational spectroscopies (adsorption and reactive sites)[1,7,10,13,24-25,37].

By combining self-organized growth on NPs on $Al_2O_3/Ni_3Al(111)$ and optical spectroscopies, we demonstrate CO-induced Pd surface diffusion from the Pd core to the Au shell in Pd/Au core/shell nanoparticles. It is reversible under low CO pressure but non-reversible after mbar CO exposure, unless nanoparticle annealing is done at 550 K (without CO), allowing recovering the initial core/shell structure. Scanning tunneling microscopy (STM), non-linear vibrational spectroscopy by sum-frequency generation (SFG) and surface differential reflectance spectroscopy (SDRS), supported by the modeling of vibrational dipolar coupling between adsorbates and nanoparticle plasmonic response, allow us following in real-time Pd diffusion to the shell surface and the impact of surface Pd:Au stoichiometry on NP plasmonic properties. We conclude that Pd dimer formation at the shell surface is favored compared to monomers under CO adsorption and Pd migration to the surface of the shell modifies the plasmonic response. We evidence also that the intense electric field enhancement by the surface plasmon resonance of the gold shell leads to a stronger SFG signal and a better sensitivity to probe CO adsorption sites. Finally, we demonstrate the possibility to control reversibly both surface stoichiometry and plasmonic response by molecular adsorption and sample temperature, opening the possibility for an active control of nanoparticle reactivity for photo-catalysis[38].

EXPERIMENTAL METHODS

Sample growth and characterization were achieved in a 5×10^{-11} mbar base pressure ultra-high vacuum (UHV) chamber. Mechanically polished $Ni_3Al(111)$ single crystal was prepared by repeated cycles of Ar^+ sputtering (15 min, 2 keV, 10 µA/cm²) and annealing at 1123 K (15 min) and then oxidized at 1143 K in a 5×10^{-8} mbar O_2 atmosphere (~90 Langmuir dose; 1 Langmuir = 1.33×10^{-6} mbar.s) to form a crystalline and strained bilayer thick alumina film. Details of the Al_2O_3 film growth are reported elsewhere[39]. Core/shell NP growth on the alumina film was done at room temperature (RT) by successive physical vapor deposition of Pd followed by Au (99.98% purity, Goodfellow, USA) using Knudsen cells at a 0.15±0.3 Å/min deposition rate. A coverage of one monolayer (1 ML) corresponds to the atomic density of Au(111) or Pd(111) planes, *i.e.* to equivalent thicknesses of 2.36 and 2.24 Å. Pd deposits from 0.05 (0.11 Å) to 2 ML (4.5 Å) and Au deposits from 0 to 11 ML (26 Å) have been explored. By this mean, the NP core size can be tuned from 0.9 to 3 nm and the shell thickness from zero up to and beyond NP coalescence when their radius becomes larger than 4.2 nm, the distance between NPs. Pd core size and geometry changes as a function of the deposited amount are reported in ref. **28**. PdAu NP size, shape and shell thickness are detailed in **Suppl. Materials** (**Table SM-1** and **Table SM-2**). NP morphology and ordering were studied with a STM microscope operating in UHV at RT (ScientaOmicron) using tungsten tips prepared by electrochemical etching in KOH. STM images were processed using WSxM software[40].

CO adsorption was monitored by sum frequency generation (SFG), a vibrational spectroscopy technique based on a second-order non-linear optical process that is only sensitive to surface thanks to the symmetry breaking occurring at the surface, leading to a non-zero macroscopic non-linear susceptibility[41-42]. In previous works, by probing CO chemisorption on Pd NPs, we have been able to attribute adsorption sites, to determine NP geometry, to study size effect over a large size range and different type of supports[28, 43] and to evidence molecule-NP charge transfer, energy relaxation and CO surface diffusion[44-45]. Since CO preferentially binds to Pd atoms rather than Au atoms at low pressure and RT, PdAu alloying in the shell and Pd diffusion can be probed not only with a high sensitivity but also in real-time. As CO adsorption is known to promote Pd diffusion in the Au shell, the surface selectivity and high sensitivity of SFG technique motivated us to investigate a wide range of pressures in order to scrutinize the segregation phenomenon. Low CO pressure allows us probing adsorption site, while upon high pressures, where structural changes happen, atom diffusion kinetic can be followed in real-time. NP annealing after CO exposition followed by CO pumping from the chamber was done to investigate temperature impact on shell composition. Hence, SFG measurements were performed at RT, in UHV condition upon CO pressure varying from 10^{-9} to 1 mbar, before and after several cycles of annealing up to 550 K. For that, we have used a 120 fs duration, 1 kHz repetition rate CPA Ti:Sa femtosecond laser (Coherent). The SFG experiment consists in overlapping in space and time on the sample two *p*-polarized collinear pulse lasers provided by the fs-laser system. The two laser pulses are a near-infrared pulse (12407 cm^{-1} wavenumber, 7 cm^{-1} width, 3 ps duration), shaped by a 4f pulse shaper and an infrared pulse (2040 cm^{-1} wavenumber, 150 cm^{-1} width, 140 fs duration) provided by a white light continuum seeded optical parametric amplifier which covers the spectral region of CO internal stretch. Prior to SFG, the sample was annealed at 523 K to desorb CO[28,43] without affecting NP ordering according to STM and literature[46].

SFG spectrum fitting method is detailed elsewhere[47]. It consists in the extraction of vibrational bands, corresponding to different CO adsorption sites. These bands are interfering with the non-resonant SFG signal arising from NPs, all of them being spectrally modulated by the IR laser (Gaussian) spectral shape. In the case of homogeneously broadened vibrational bands, the visible spectral width is considered to be small compared to the vibration bandwidth and SFG spectra fitting is done using **Eq. 1**:

$$SFG(\omega) = IR(\omega)\left|\chi_{NR}^{(2)}e^{i\phi} + \sum_q \frac{A_q}{\omega-\omega_q+i\Gamma_q}\right|^2 \qquad \textbf{Eq. 1}$$

$\chi_{NR}^{(2)}$ is the non-resonant second-order macroscopic susceptibility arising from the metallic surface, called non-resonant signal (NR), with a phase difference ϕ relative to the second term, which corresponds to the sum of macroscopic non-linear susceptibilities of the different vibrational states, assumed to have a lorentzian lineshape. For each vibration q, A_q is its amplitude, proportional to molecular surface coverage, ω_q is its central frequency and Γ_q is its half-width at half-maximum.

The change of surface reflectivity in the UV-Vis range was followed in real-time during the growth of Au on the Pd NP array, by surface differential reflectance spectroscopy (SDRS). The experimental set-up and principle are described elsewhere[48-50]. SDRS can be used to identify localized surface plasmon resonance (LSPR) of metallic NPs[48-49]. Briefly, the specular reflection of an un-polarized light of a deuterium/halogen lamp (photon energy from 1.1 to 5 eV) focused at the sample surface at 45° of incidence, was recorded by a low-noise fibered spectrometer (Ocean Optics) and normalized by the signal of the reference surface prior to the growth. A signal to noise ratio better than 10^3 can be achieved after the correction from lamp drift and dark signal, for a 10 sec acquisition time (200 averaged spectra of 50 ms duration). The CO adsorption was similarly monitored by SDRS to deduce how NP composition change affect the plasmonic properties.

COMPUTATIONAL METHODS

Modeling of the vibrational coupling

Dipole-dipole vibrational coupling calculation between CO adsorbed at the NP shell surface is based on a classical electrostatic model developed for CO on single crystal surfaces[51-52] and adapted from our previous works on Pd(100) single crystal[53] and MgO supported Pd NPs[43]. In order to account for various adsorption phases and different adsorbate distances within the same adsorbate layer, dipolar interactions must be calculated for each molecule and the spectrum be summed over all molecules. SFG spectra are calculated according to the formalism of Cho *et al.*[54] to obtain the perturbed second-order susceptibility $\chi^{(2)}_{i,j}(\omega)$ for each CO molecule at position {i, j} on the surface.

$$\chi^{(2)}_{i,j}(\omega) = \frac{\chi^{(2)}_R(\omega)}{[1+\alpha(\omega)\,U_{i,j}][1+\alpha_e\,U_{i,j}]^2} \qquad \textbf{Eq. 2}$$

where $\chi^{(2)}_R(\omega)$ is the molecular nonlinear susceptibility (*i.e.* the second term in **Eq. 1** in the absence of dipolar coupling) while the denominator accounts for electric field corrections induced by dipolar coupling. It is composed of three terms having the general form $[1+\alpha\,U_{i,j}]$ for each of the three wavelengths (SFG, near IR, IR). $U_{i,j} = \sum_{m,n\neq i,j} u_{m,n}$ is the summed dipolar perturbation produced by surrounding molecules, where $u_{m,n}$ is the dipolar interaction potential of a single neighbor molecule $\{m,n\}$[55-56]. $\alpha(\omega)$ is the molecular polarizability that has a Lorentzian shape centered at the CO singleton frequency for the considered site, shifted from the coverage dependent chemical contribution induced by chemisorption[53-57]. $\alpha(\omega)$ depends on the electronic polarizability α_e= 3 Å^3 and the vibrational polarizability α_υ a fitting parameter ranging from 0.1 to 0.3 Å^3 [53,56-57]. Because ω_{nearIR} and ω_{SFG} are far from vibrational resonances, then $\alpha(\omega) = \alpha_e$. Different PdAu(111) alloy surfaces with isolated Pd monomers ($Pd_{0.33}Au_{0.66}$) and dimers ($Pd_{0.4}Au_{0.6}$) are considered, for different CO coverages (0.33/0.5 ML for monomers - 0.2/0.4 ML for dimers).

Modeling of the plasmonic response

Numerical simulations using the wave optics electromagnetic module of COMSOL Multiphysics have been done to model un-polarized SDRS ΔR/R spectra in the UV/Vis range for various NP shapes, sizes and compositions. It consists in solving the differential form of Maxwell equations by finite-element method, together with material laws for propagation in various media, to calculate the electromagnetic field distribution in 3D. The wavelength analysis is performed from 200 to 1200 nm (step of 10 nm) corresponding to a 1-6 eV photon energy range. The overall surface reflection coefficient is calculated by integrating the power flux emitted through the output port. Considering the periodicity of the semi-infinite nanostructured surface, the smallest unit cell is defined in agreement with the $\left(\sqrt{67}\times\sqrt{67}\right)R12.2°$ reconstruction phase of the alumina oxide[26,58] and Floquet periodic conditions are applied at the boundaries to insure continuity. Incident angle is set at 45° on the input port for both incident transverse electric (TE) and transverse magnetic (TM) electromagnetic waves. Perfectly matched layers placed at the top and bottom of the unit cell avoid the artificial creation of a Fabry-Perot cavity leading to back-reflection from the far field that could modulate the simulated spectrum. The differential reflectivity spectrum is obtained by averaging TE and TM differential reflectivity for an un-polarized beam:

$$\frac{\Delta R}{R}=\frac{R(t)-R(t=0)}{R(t=0)}=\frac{R(t)}{R(0)}-1=\frac{R_{TM}(t)+R_{TE}(t)}{R_{TM}(0)+R_{TE}(0)}-1 \qquad \textbf{Eq. 3}$$

$R(t=0)=R(0)$ is the reflectivity of the surface without gold at t=0, *i.e* the Pd NP array on the alumina film on $Ni_3Al(111)$ without gold and $R_{TM,TE}(t)$ is the reflectivity as a function of time during the gold evaporation on the surface for TM or TE polarization. In the model and in agreement with experimental observation, gold is growing around Pd NP only and not on the alumina. The E_{field} distribution at nanoscale helps us to identify LSPR around the NP and assign them to the different spectral features in the $\Delta R/R$ spectra. In agreement with STM results, different PdAu geometries have been considered from half-sphere to half-ellipsoid or large hexagonal NP to account for NP coalescence observed in the case of large Au deposited amounts. More details can be found in **Suppl. Materials** (**Figure SM-1**). Considering the small dimension of nanostructures, a mesh size ≤ 1 nm is required to describe correctly the interface, while for the vacuum and the substrate, a < λ/10 mesh size at 6 eV is used (16 nm). Different Pd core sizes have been considered and a PdAu alloy has been used for the core/shell interface or the shell surface in agreement SFG findings. Macroscopic dielectric functions or Ni_3Al, Al_2O_3, Pd and Au provided by COMSOL's in-built material library are used for the substrate, alumina layer, Pd core and Au shell respectively. For the PdAu alloy, an effective dielectric function is calculated by a linear combination of Pd and Au dielectric function weighted by their relative concentration[59].

RESULTS AND DISCUSSION

Surface topography

In **Figure 1a-d** are presented 25x25 nm^2 STM images of Pd/Au NPs for different Au deposits of 0, 2.1, 8.5 and 17.9 Å on a 3 nm large Pd core (equivalent thickness 4.48 Å), corresponding to relative average concentrations in the NP of Pd_1Au_0, $Pd_{0.68}Au_{0.32}$, $Pd_{0.34}Au_{0.66}$, $Pd_{0.2}Au_{0.8}$. Pd nucleate and grow at the periodic defect sites of the alumina film leading to an hexagonal lattice of 4.2 nm period[26,28]. Pd NPs act as seeds for the further growth of Au. In agreement with the literature, gold grows on the Pd core to form a core/shell structure. However, ordering and density of NPs rapidly decay above 2.1 Å of Au deposit (**Figure 1e**) or 1 ML Au shell according to literature[60]. The initial stage of coalescence consists in the merging of two adjacent NPs (**Figure 1b**). As Au growth continues, objects with a larger aspect ratio result from the multiple coalescence of 3-4 (**Figure 1c**) and 6-9 NPs (**Figure 1d**) for 8.5 and 17.9 Å Au deposits, respectively. Topography profiles in **Figure 1f** illustrates how this coalescence takes place. NP shape can reasonably be approximated to a half-sphere in the early Au growth stage; it progressively evolves to a half-ellipsoid with increasing aspect ratio and finally to a flat polygonal NP, that can be approximated by a regular hexagon. Such shapes have been used to model the UV/Vis surface reflectivity.

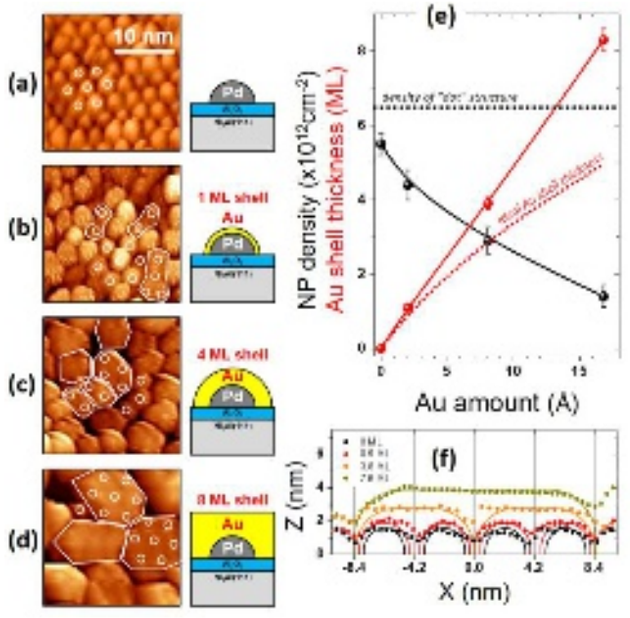

Figure 1. (a-d) 25x25 nm^2 STM images (U_b=1 V, I_t=12 pA) of Pd/Au NPs for 3 nm large Pd core and increasing Au deposits of 0, 2.1, 8.5 and 17.9 Å corresponding to 1, 4 and 8 atomic layers of Au in the shell. White circles stand for the initial nucleation sites. A sketch of the core/shell NPs is given for each case. (e) NP density and estimated shell thickness for increasing Au deposit. The "ideal case" refers to an array

of identical core/shell NPs where no coalescence has occurred. (f) Topography profiles from STM images with the estimated shape of individual or coalesced NPs highlighted by the continuous lines.

The Au shell thickness can be derived from the NP density, Pd/Au NPs and Pd core shapes[28]. Considering the decrease of NP density from 5.5 to 1.2x10^{12} NPs/cm², the Au shell thickness raises quasi-linearly with the Au deposited amount, faster than the ideal case of a half-sphere geometry. The estimate of shell thicknesses and NP sizes as a function of Au deposit for various Pd core sizes for an ideal half-sphere are given in **Table SM-1** and **Table SM-2**. For half-sphere, the coalescence is expected for 8.8, 12.8 and 13.2 Å deposits of gold on 3, 1.4 and 0.9 nm large core. Shell thicknesses are estimated around 0.9±0.2, 3.6±0.9 and 8.2±2 ML, for 2.1±0.5, 8.5±2 (coalescence) and 18±4 Å (above coalescence) Au deposits respectively on a 3 nm large Pd core. A sketch of the corresponding core/shell NP is given for each case in **Figure 1**, where the shell thickness has been approximated to 1, 4 and 8 ML afterward in the article. A similar trend was observed for intermediate Pd core size (1.4 nm) and smaller Pd core (0.9 nm), but the coalescence of NP is reached for higher deposit of gold (**Tables SM-1** and **Table SM-2**).

Impacts of CO adsorption on NP atomic structure

In **Figure 2** are reported SFG spectra at RT, with their corresponding fit obtained under three representative CO pressures (10^{-8}, 10^{-3} and 1 mbar) on four different systems: 3 nm Pd core without and with gold shell (1, 4 and 8 ML). The complete series of SFG spectra have been recorded from 10^{-8} to 1 mbar (**Figure SM-2**). The SFG spectrum is composed of vibrational bands of adsorbed CO, interfering with a non-resonant (NR) response of the metallic surface spectrally modulated by the Gaussian IR laser. Both are impacted by CO pressure and Au shell thickness. For bare Pd core (**Figure 2a-c**), CO binds to Pd atoms in different configurations depending on the CO pressure and coverage: (i) bridge sites (red band on (111) facets and orange band on (100) facets from 1890 to 1980 cm^{-1}), (ii) linear sites on facets (blue band at ~2090 cm^{-1}), and at NP edges ~2060 cm^{-1} (olive band). A (grey) band at ~2010 cm^{-1} has been observed and previously attributed to CO binding at alumina defects[28].

Already for a single monolayer Au shell, CO binding behavior radically changes (**Figure 2d-f**). At low CO pressure (10^{-8} mbar), CO adsorption is much lower than for bare Pd core. Concerning bridge CO, the red band is absent while the orange band has strongly decreased. Two weak bands are observed, one at 2065 cm^{-1} (light green), at a similar frequency than CO on Pd edges (olive) but with a significantly narrower bandwidth and one at 2077 cm^{-1} (dark cyan). At intermediate pressure (10^{-3} mbar), the light green band is replaced by a new band at 2042 cm^{-1} (violet) and the dark cyan band has increased. In the mbar range, the violet band is not observed anymore, while the dark cyan band now dominates the spectrum and a new band is visible at 2120 cm^{-1} (yellow). At 4 ML shell thickness (**Figure 2g-i**), similar bands but with a weaker intensity are

observed at low CO pressure while the non-resonant signal dominates the SFG signal. Again, at intermediate pressure, the violet band dominates the spectrum with a comparable intensity than for 1 ML shell NPs. In the mbar range, a very similar spectrum compared to 1 ML shell is obtained, with an intense dark cyan band accompanied with small violet and yellow bands.

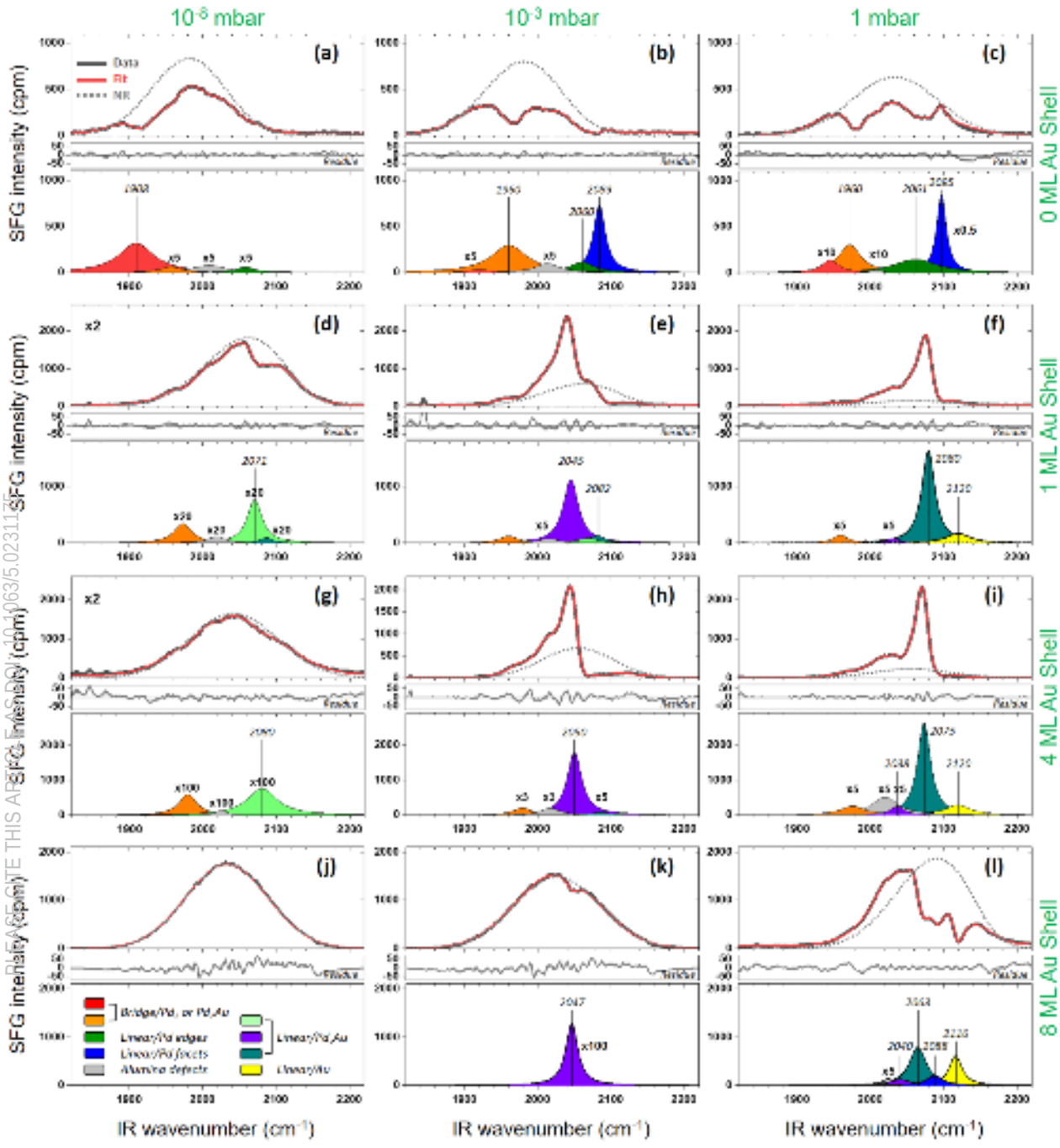

Figure 2. SFG spectra (black) at room temperature for three CO pressures (10^{-8}, 10^{-3} and 1 mbar) for 3 nm Pd core covered by 0 (a-c), 1 (d-f), 4 (g-i) and 8 ML (j-l) thick Au shells. For each spectrum, data, fit and deconvoluted NR signal are given in the upper panel, the residue in the middle panel and deconvoluted CO bands in the lower panel. Band attribution to CO adsorption sites are indicated in (j) panel. As indicated, multiplication coefficients have been applied to highlight some bands as well as spectra (d) and (g).

Finally, at 8 ML shell thickness (**Figure 2j-l**), CO adsorption is no longer observed at low pressure. At intermediate pressure, the weak violet band becomes visible and at mbar pressure, dark cyan and yellow bands dominate the spectrum, while violet is much smaller, the orange band is absent and a new band (blue) at 2090 cm^{-1} has appeared. By increasing further the pressure at 3 mbar (not shown here), the dark cyan band strongly increases. Notice that the NR intensity decreases with CO pressure for all shell thicknesses above the threshold pressure of 10^{-3} mbar but is less affected by CO adsorption for the thickest shell. The phase difference between NR and CO resonant vibrations increases with CO coverage while it decreases with the shell thickness (**Figure SM-3**).

A first conclusion can be made about the shell composition. At CO pressure lower than 10^{-3} mbar, the shell (1 to 8 ML thick) is mostly composed of gold, showing the higher stability at 300 K of gold on the Pd core surface. This is in agreement with the results of the group of H.-J. Freund on Au/Pd catalysts, where both metals were co-deposited in vacuum condition[25]. They have demonstrated a higher stability of Au atoms at the NP surface at RT. Gold atoms segregate to the surface and prefer to stand at the edges of AuPd alloy NP.

According to the literature, the yellow band ~2115 cm^{-1} is assigned to CO binding at Au atoms; it is only present above 10^{-3} mbar CO pressure (**Figure SM-4**) owing to the low CO adsorption energy on gold at RT[25,61]. Incidentally, it confirms the presence of remaining gold atoms at the NP surface. The frequency is characteristic of low coordinated adsorption sites on Au, suggesting that CO first binds to Au at edges rather than on Au at facets[24]. The full coverage of the core and the growth of the shell is also confirmed by the reduced sensitivity of the NR signal to CO adsorption and the decrease of the phase difference. Indeed, non-linear susceptibility is much larger for Au than for Pd while the phase is lower. The orange band, observed on 1 ML Au shell and at smaller intensity on 4 ML shell, has a frequency too high for CO bridged on Pd facet encountered at 1920 cm^{-1} at this pressure. In the literature, this band was attributed to bridged CO on Pd dimers surrounded by Au atoms, also confirming that the Au shell covers almost completely the Pd core. The presence of two bands (light green and dark cyan) at 2065±3 and 2077±3 cm^{-1} are in a good agreement with reported results on alloyed single crystal or nanoparticles[7,10,24]. On NP, they were assigned to CO binding on-top of isolated Pd atoms in the gold shell, on NP facets and edges, respectively. The increase of the dark cyan band at high pressure suggests that Pd segregates to the surface, in agreement with literature. The changes of SFG phase difference with CO pressure can also be related to Pd segregation to the surface. Indeed, at low CO pressure, the phase is around 1.6 rad and raises up to 2.9 rad as CO binds to Pd atoms that have migrated to the surface (**Figure SM-3**). However, the origin of violet band and its presence only at intermediate CO pressure remains unclear in the literature[10,24]. Scrutinize it could give a better picture of the segregation mechanism, as discussed later.

In vacuum, Pd atoms tend to stay in the bulk of core/shell Pd/Au NPs[25] due to the lower surface energy of gold than that of palladium[62]. It is now well admitted that under CO adsorption, Pd segregation towards the Au shell surface can occur and stable Pd monomers and even dimers can be formed at edges and facets[24]. We can do several general remarks from **Figure 2**. At relatively low CO pressure (<10^{-3} mbar), where Pd segregation is reduced, the progressive disappearance of CO/Pd band for thicker shell shows that the Pd core can be passivated by increasing the gold shell thickness. The Pd diffusion length in the shell can be estimated around 2-3 ML. However, in the mbar pressure range, Pd diffusion to the surface can be triggered by CO up to 8 ML. The similarity of SFG spectra for 1 and 4 ML shell in the mbar range indicates a similar composition of the surface. It means that the core can provide enough Pd atoms to reach the same surface stoichiometry. Nevertheless, the small amount of bridge CO suggests that Pd concentration in the shell remains low enough to limit the formation of large Pd domain in the shell. Similar observations have been made for AuPd single crystal[13] and supported AuPd nanoparticles[21,24]. Consistently with Pd(100)[53], Pd(111) single crystals[63] and Pd NP[28,64] on alumina thin films, hollow CO are not observed by SFG at room temperature and cannot be used to probe the extension of Pd domains in the Au shell.

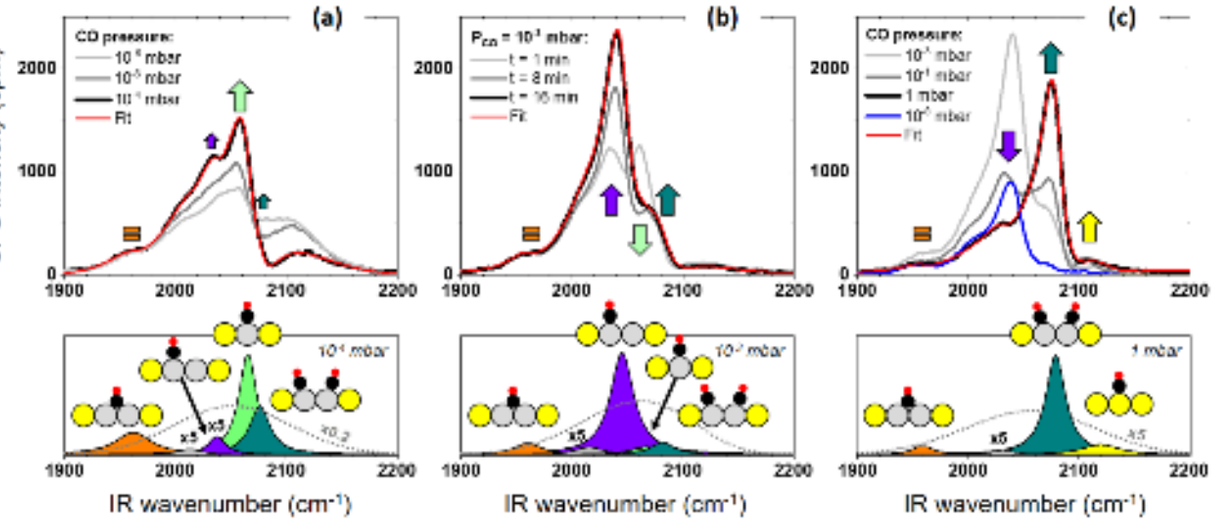

Figure 3. SFG spectra of CO adsorbed on 1 ML Au shell on 3 nm Pd core at RT for different CO pressure ranges: (a) from 10^{-8} to 10^{-4} mbar, (b) at 10^{-3} mbar during 16 min, (c) from 10^{-3} to 1 mbar and then back to 10^{-8} mbar. Fitted CO bands are given below each series for 10^{-4}, 10^{-3} and 1 mbar as well as in inset suggested adsorption sites for these bands.

A closer inspection on the impact of CO pressure on binding sites for 1 ML Au shell (**Figure 3**) helps understanding the diffusion mechanism. Suggested CO adsorption sites schemes are given in inset and are discussed later. For CO pressure lower than 10^{-4} mbar, the light green band (CO/Pd monomers on facets) is present and CO coverage at these sites can be tuned reversibly by changing CO pressure (**Figure SM-2**). Above this threshold pressure, the violet band (2045 cm^{-1}) appears and replaces CO/Pd monomers on facet, while

CO/Pd monomers at edges do not seem to be affected (**Figure 3a**). At 10^{-3} mbar, the increase over several minutes of the violet band can be followed in real time, as a sign of Pd enrichment of the shell. The band intensity rises as CO coverage increases, while the frequency blue-shifts due to larger dipolar coupling between adsorbates (**Figure 3b**). After PdAu alloying in the shell, decreasing the CO pressure down to 10^{-8} mbar does not allow recovering the initial core/shell structure of the NP contrary to $Pd_{70}Au_{30}$ single crystal[9]. Only the violet band is present with a lower intensity and the orange band (bridge CO/Pd dimers) which has a larger intensity than before alloying (blue curve in **Figure 3c**). However, starting from the alloyed surface, new cycles of CO pressure in the same range shows a reversible CO adsorption as observed by Toyoshima *et al*.[9]. At pressure higher than 10^{-3} mbar, CO population switches from the violet band back to the dark cyan band. We deduce that no significant structural change occurs in the mbar range, since decreasing the pressure back to 10^{-8} mbar leads to the same spectrum obtained after the surface alloying at 10^{-3} mbar (blue curve in **Figure 3c**). For a 4 ML thick Au shell, a very similar behavior is observed with an irreversible transition at 10^{-3} mbar. For 8 ML Au shell, as Pd segregation is harder to achieve, an equivalent transition is observed in the 0.1-1 mbar CO pressure range (**Figure SM-2**).

A band at 2040 cm^{-1} (similar to the violet band) was observed on TiO_2[10] and alumina[24] supported PdAu NPs at low CO pressure after exposure to CO and O_2 mixture in the mbar range. Thus, this band is likely CO strongly bound at the shell surface on Pd atoms. DFT calculations have suggested that it could originate from CO binding to Pd monomers having a lower coordination to surrounding Au atoms due to the subsurface migrating of Pd close to the absorption site[24]. However, this hypothesis seems in contradiction with SFG results. Indeed this band has a higher intensity for 4 ML Au shell than for 1 ML shell thickness where the amount of Pd in the first subsurface layer is obviously larger. More, the light green band at 2065 cm^{-1} (CO on Pd monomers) would be significantly shifted for 1 ML gold shell, due to the presence of subsurface Pd, compared to thicker shell, which is not the case. It was also proposed that one or two CO adsorbed at Pd monomers could be responsible for Pd segregation leading to the formation of Pd dimers on facets and edges with an equivalent stability than on facets, but very unlikely to Pd trimers[24]. Three adsorption configurations can then be encountered on the dimer: 1 CO bridged on two Pd, 1 CO on-top on one of the Pd, and 2 CO on-top on each Pd or one Pd. The signature of bridge CO on dimers is expected around 1950 cm^{-1} (orange band) and has not increased with the appearance of the violet band excluding bridge CO to be the candidate. Then, only on-top CO (1 or 2) per Pd atom of the dimer should be considered. It is important to notice that the transient violet band is not observed when pressure is raised fast from 10^{-4} to the mbar range. However, the shell is also modified in an irreversible way. It demonstrates that this structural transition can happen very fast. The narrow range of CO pressure at which the violet band can be observed could explain why it was not reported in the literature that most of the time focus either on very low pressure or on the mbar range.

Mechanism of Pd segregation and band assignment

We propose that the band at 2045 cm^{-1} involves Pd dimers that play a crucial role in the mechanism of Pd segregation to the shell surface. Three different scenarii sketched in **Figure 4**, starting from CO on top of Pd monomer (light green band in SFG), can be suggested. They are based on our experimental findings and literature results[9,19,21,24].

(a) At 10^{-3} mbar, migration of core Pd to Pd monomers to form dimers is triggered by CO adsorption. Here, the violet band would be attributed to 2 CO molecules per Pd dimer. At higher pressure, the disappearance of the violet band to the benefit of the dark cyan band (CO on Pd monomer at edges), may be explained by CO assisted Pd diffusion at the shell surface. CO binding on first neighbor sites are represented with a small tilt angle to account for electrostatic repulsive forces as it was deduced from DFT calculation in a previous work on Pd(100)[53]. Repulsive forces between molecules split Pd dimers into two Pd monomers that can migrate to edges contributing to the increase of the dark cyan band, as suggested by Zhu *et al.*[24] Decreasing back the CO pressure should lead to a lower coverage of CO on Pd monomers and a frequency back to 2065 cm^{-1} and not at 2045 cm^{-1} as it is observed. Only a back diffusion of Pd to form again dimers would be consistent. However, if Pd dimers are more stable than monomers, the latter should not be observed at low pressure. Considering these contradictions, the first scenario is not able to attribute clearly the 2045 cm^{-1} band.

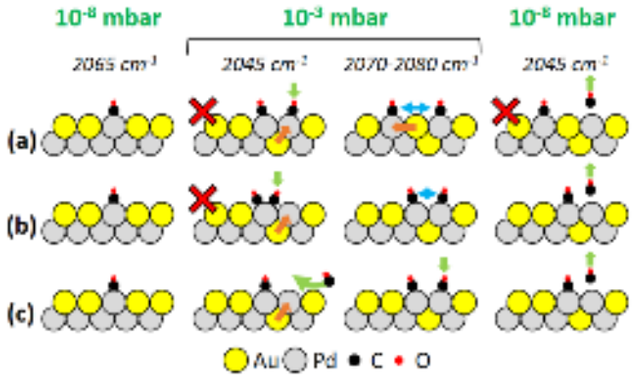

Figure 4. Three suggested scenarii to attribute the violet band at 2045 cm^{-1} and the reversible kinetics of Pd segregation with CO pressure on 1 ML Au shell. Red crosses indicate unlikely situations for the violet band. Green arrows stand for CO adsorption from the gas phase, orange arrows for Pd that have migrated to or along the surface and replaced by an Au atom. Blue arrows indicate dipolar interactions between molecules. First neighbor CO are represented with a tilt angle induced by electrostatic repulsive forces[53].

(b) In ref. **18**, multiple CO adsorptions on single Pd atoms at NP vertex sites have been considered in the description of CO-adsorption-driven mechanism leading to the Pd segregation to the shell. Based on this hypothesis, in this second scenario, at 10^{-3} mbar, 2 CO adsorbed on a single Pd lead to Pd segregation and the formation of a dimer. Here, 2 CO on a single Pd should correspond to the violet band. As soon as this new site appears, one CO migrates to the next Pd to reduce steric hindrance. In this new configuration, CO frequency blueshifts to 2070-2080 cm^{-1}. By decreasing CO coverage (pressure), only one CO remains on-top on dimers with a frequency at 2045 cm^{-1}, which is not consistent with the previous assumption for this band (2 CO on 1 Pd). The frequency of 2 CO on a Pd monomer is very unlikely expected at 2045 cm^{-1} due to larger dipolar interactions, but rather closer to 2100 cm^{-1}.

(c) In the third scenario, at 10^{-3} mbar, transient CO adsorption on Au atoms leads to Pd segregation and formation of dimers either from a Pd monomer or by the segregation of a Pd dimer as discussed later. As pressure remains low, only one Pd is occupied (violet band) while at higher pressure, CO molecules occupy both Pd. The pressure (coverage) can then reversibly decreased with one CO per Pd dimer with a frequency at 2045 cm^{-1}. Similarly to what suggests this scenario **(c)**, on $Pd_{70}Au_{30}(111)$ alloy surface, CO coverage can be tuned in a reversible way from bridge coordination on Pd dimers at low CO pressure to on-top coordination at higher pressure[9]. However, DFT modeling[24] has shown that 1 CO on-top on one Pd of the dimer has a similar frequency than on a monomer around 2075 cm^{-1} and not 2045 cm^{-1}. It was also shown that on PdAu alloyed surface, the 2080 cm^{-1} band is more stable and was attributed to CO on-top on an isolated Pd as well as CO on-top on a Pd adjacent to a next nearest neighbor Pd, a Pd dimer[37]. Both are in contraction with scenario **(b)** and **(c)**. However the expected blueshift due to dipolar interaction by doubling CO coverage on Pd dimer is compatible with the 30 cm^{-1} difference between the violet and the dark cyan bands, by analogy with CO/Pd(100)[43,53].

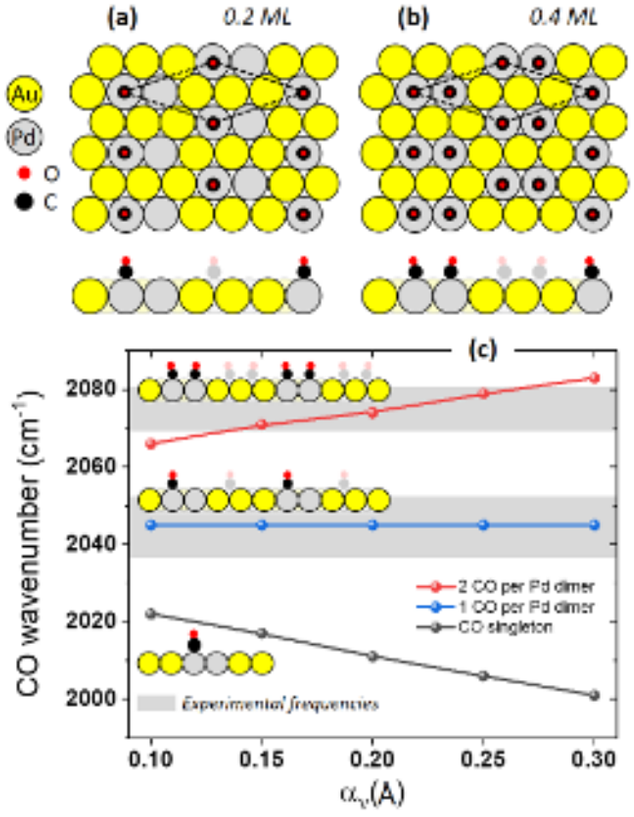

Figure 5. CO adsorption phases on $Pd_{0.4}Au_{0.6}$ surface with (a) 0.2 ML (1 CO per Pd dimer) and (b) 0.4 ML CO coverage (2 CO per Pd dimer). (c) CO band wavenumber of previous phases and of CO singleton on Pd dimer, including dipolar coupling and at higher coverage as a function of vibrational polarizability.

In order to determine the most probable scenario, we have conducted dipole-dipole vibrational coupling calculations between CO adsorbed at the surface of the NP shell. The impact of adsorption site, site coordination and molecular coverage on the CO internal stretch frequency was investigated. In particular, we have calculated the impact of dipolar coupling on the CO frequency for 1 or 2 CO per Pd monomer and dimer. $Pd_{0.33}Au_{0.67}$ and $Pd_{0.4}Au_{0.6}$ stoichiometry can be reached if considering only isolated Pd dimers and monomers, respectively in the shell. These values are lower or equivalent than the NP stoichiometry for 1 ML ($Pd_{0.68}Au_{0.32}$) and 4 ML ($Pd_{0.34}Au_{0.66}$) Au shell, respectively. Those surface stoichiometries can reasonably be considered for 1 and 4 ML shells and have been used in the dipolar model. The details of surface structure and the considered adsorption phase are given in **Figure 5(a-b)** for Pd dimers and in **Figure SM-5** for Pd monomers. First neighbor CO are represented with a tilt angle induced by electrostatic repulsive forces, but tilt angle was not included in the model. For 8 ML Au shell, the stoichiometry is limited to the one of the NP ($Pd_{0.2}Au_{0.8}$): the dilution of the Pd core in the Au shell leading to an evident decrease of available Pd monomers and dimers on the surface as evidenced in SFG spectra. The consequence is a lower dipolar interaction between monomers or dimers. We have used standard values of 3 Å^3 for the electronic

polarizabilities of CO on Pd, while the vibrational polarizability was tuned from 0.1 to 0.3 Å^3, an acceptable range[43,53]. Depending on the polarizability, the vibrational frequency of a single CO on Pd (without dipolar coupling) was adjusted from 2001 to 2022 cm^{-1} to fit with the observed 2045 cm^{-1} band at low coverage (0.2 ML). By doubling CO coverage to 0.4 ML (two CO per dimer), the band shifts to 2075±10 cm^{-1}, depending on the vibrational polarizability (**Figure 5c**). These values are in a very good agreement with SFG results that can validate scenario **(c)** considering Pd dimer with a single CO at low coverage (after Pd segregation) and two CO at higher coverage. In scenario **(b)**, also reported in ref. **18**, two CO binding per Pd monomer were suggested to explain Pd segregation. Results of dipolar calculations for this case are given in **Figure SM-5**. They show that doubling CO coverage leads to a CO frequency around 2095±15 cm^{-1}. This band was observed only for 8 ML Au shell in the mbar range, suggesting their low stability considering the strong electrostatic repulsion between CO. Hence, these sites are likely not involved in Pd segregation occurring around 10^{-3} mbar.

In the literature, the increase of the 2077 cm^{-1} band (dark cyan in SFG) at higher CO pressure was associated to Pd segregation to the surface forming monomers and dimers at edges[24]. We propose here a different scenario **(c)** where Pd dimers play the most important role. As evidenced by SFG, around 10^{-3} mbar, CO adsorption becomes possible on gold at RT (**Figure SM-4**). The transient adsorption of CO probably increases surface energy, leading to Pd segregation close to Pd monomer, forming a dimer. CO band shifts at lower frequency (violet band) as Pd dimers replaces Pd monomers. When the CO coverage increases (2 CO per Pd dimer), CO frequency shifts to higher frequency due to larger dipolar coupling, evidenced by the replacement of the violet band by the dark cyan band in SFG spectra. However, for a 4 ML Au shell the amount of Pd monomer at low CO pressure is rather low compared to a 1 ML Au shell, while the CO band on dimers is similar at intermediate pressure. More, CO on Pd monomers are inexistent at 8 ML and only CO on dimers appears when Pd starts to segregate. This difference clearly evidences that Pd dimers are segregating through a thick shell and not monomers.

Plasmonic response of PdAu nanoparticles

SDRS was used to follow the gold shell growth kinetic through the evolution of the surface optical response and more specifically here, the LSPR of the gold shell. In **Figure 6a-b** are shown the spectra of the reflectivity changes (ΔR/R) for increasing Au deposits from 0 to 26 Å of Au on 1.4 and 3 nm large Pd cores, corresponding to 10 and 7 ML Au shell thickness, respectively. The sum of reflectivity (R), absorption (A) and transmission (T) at an interface equals 1. A sketch of each considered system is given in the inset for 1 ML thick shell in order to highlight that the two systems will reached NP coalescence for different shell thickness.

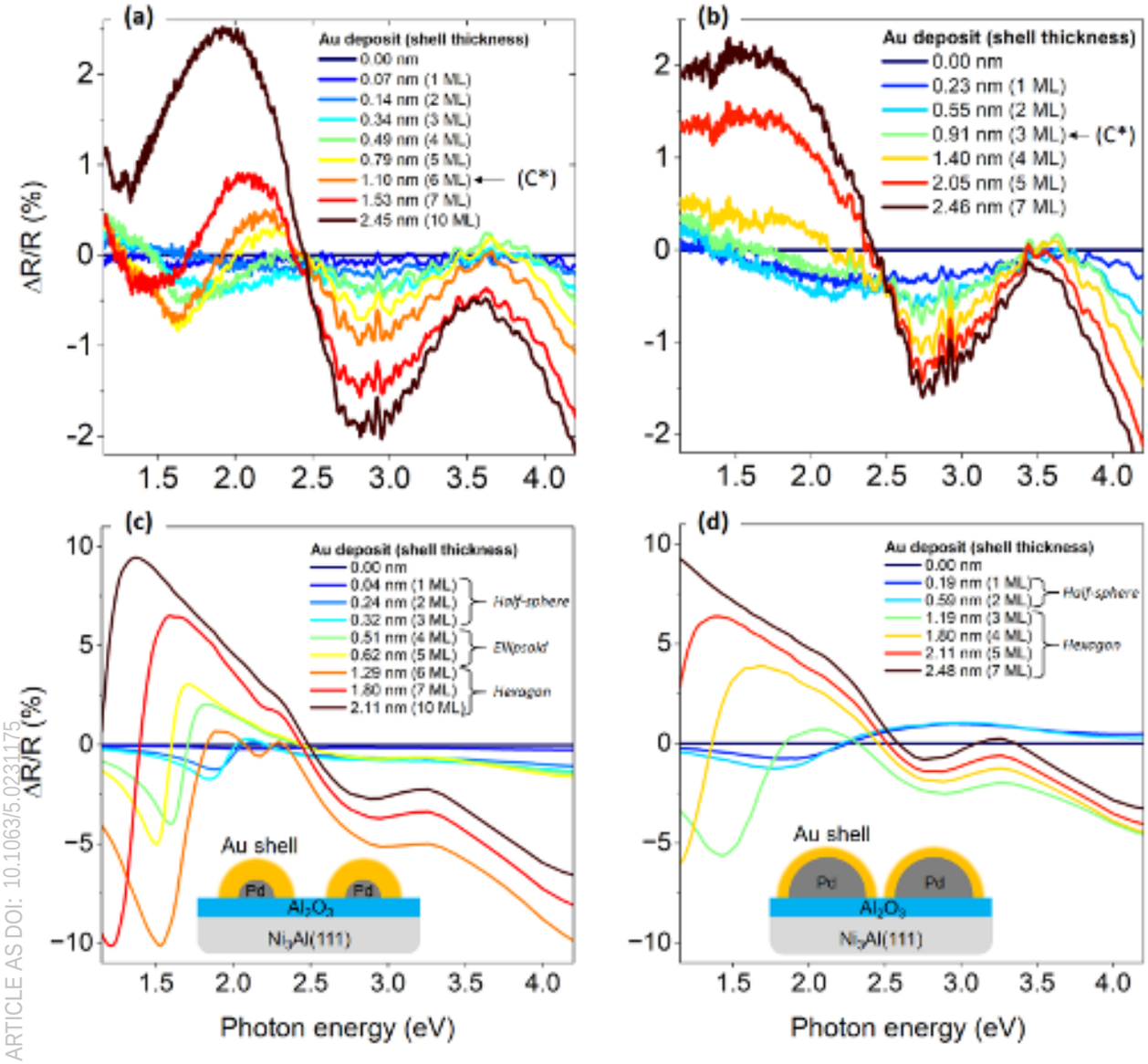

Figure 6. Experimental (a, b) and simulated (c, d) differential reflectance spectra (ΔR/R) for Pd core sizes of (a, c) 1.4 nm (0.45 Å of Pd) and (b, d) 3 nm (4.5 Å of Pd), as a function of Au deposit of equivalent thickness ranging from 0 to ~25 Å. Corresponding shell thickness and coalescence are indicated (C*). In each inset, a representation of the system.

For both Pd cores, three common features are observed. (i) A negative differential reflectance above 2.5 eV due to gold interband transition[65]. (ii) A positive differential reflectance below 2.5 eV due to a higher reflectivity of Au than Al_2O_3/Ni_3Al. (iii) The presence of an isosbestic point in the spectra series at 2.5 eV close to the expected LSPR of spherical gold nanoparticles (2.3 eV). Three major differences are also evidenced as Pd core size decreases: (i) the intensity increase of interband transitions and (ii) the presence of broad absorption features shifting from 2 to 1.1 eV and (iii) the energy of the isosbestic point shifting from 2.3 to 2.5 eV. Nevertheless, the attribution of this absorption band to the shell LSPR is not straightforward. Indeed, light reflection from vacuum (n=1) on a plasmonic surface does not allow to couple light to the SPR because the photon k momentum is always larger than surface plasmon *k* momentum. However, in the case of a

nanoparticle, because of the effective index of the NP layer and the inhomogeneity of the electric field distribution, it is possible to match plasmon momentum and couple to it without requiring an excitation from a high index medium[66]. This absorption band becomes distinguishable starting from a gold shell thickness of 3 ML for a small Pd core of 1.4 nm, while for a large Pd core (3 nm) it is almost not visible and appears only after nanoparticle coalescence (**Figure SM-6**). It is concomitant with SFG results that have evidenced a Pd-Au alloy at the shell surface.

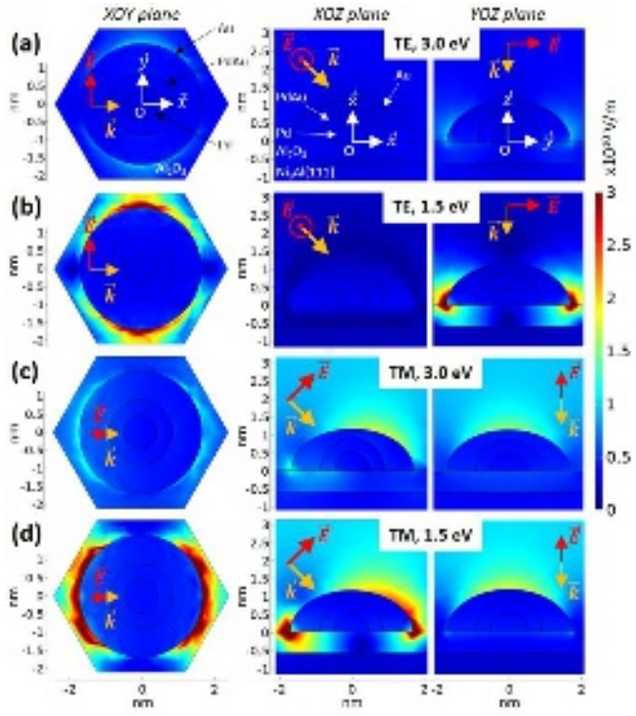

Figure 7. Electric field distributions in the surface plane (left), the incidence plane (center) and perpendicular to it (right) for TE polarization at (a) 3 eV and (b) 1.5 eV and TM polarization at (c) 3 eV and (d) 1.5 eV photon energy for a 1.4 nm Pd core covered by 2 ML PdAu half-sphere shell and 2 ML Au shell half-ellipsoid Au shell.

Numerical simulations of ΔR/R spectra by finite-element-method are plotted and compared to experimental SDRS data in **Figure 6c-d** for similar core sizes, increasing Au deposits and NP geometry ranging from half-sphere to half-ellipsoid and large flat regular hexagons (**Figure SM-1**). Calculations are qualitatively in a good agreement with experimental data. Interband transitions above 2.5 eV as well as the important ΔR/R changes depending on core size and shell thickness at lower photon energy are both fairly well reproduced. For small and average core sizes, we can attribute the strong absorption band shifting from 2 to 1 eV depending on Au quantity, to the localized surface plasmon resonance of the Au shell. It is confirmed by the electric field distribution for TE and TM polarizations calculated at 3 and 1.5 eV for a 1.4 nm Pd core covered by 2 ML PdAu half-sphere shell and 2 ML Au shell ellipsoid Au shell (**Figure 7a-d)**. For a TE-

polarization, a large field enhancement occurs parallel to the surface around the NP around 1.5 eV. It is resulting from LSPR coupling between NP. For a TM-polarization, due to the 45° incident angle of incoming light, half of the light polarization is projected along the surface plane that leads to the excitation of the in-plane plasmon mode and the other half can excite the out-of-plane plasmon mode. It remains relatively weak compared to the plasmon mode parallel to the surface (**Figure 7d)** and does not change as radically with photon energy as for TE-polarization. The intensity difference accounts for the smaller Au quantity in the sample normal direction and for the larger oscillator strength in the surface plane direction.

However, for large core, no clear LSPR is observed in experimental $\Delta R/R$ signals, also confirmed by the numerical calculations. The simulation (not shown) shows a rapid disappearance of the LSPR because of the NP coalescence above 3 ML Au shell, where the plasmonic response barely starts. Despite the good agreement, important differences are observed like: (i) the absolute value of $\Delta R/R$ changes, (ii) the LSPR bandwidth, (iii) the intensity ratio between LSPR and interband transition and (iv) no LSPR is observed for 1 and 2 ML Au shell thickness by SDRS, in agreement with SFG (Pd-Au alloy), on contrary to the model. The fully classical treatment used by COMSOL to compute the reflectivity and the use of macroscopic dielectric function of alumina, palladium and gold could explain the intensity changes (i) and also the bandwidth difference (ii) as finite-size effect are not accounted for[48]. The size/shape dispersion, not included in the model can account for differences (ii) and (iii). Indeed, mixing results from different size configurations helps to broaden the LSPR band and weaken its intensity relatively to interband transitions. Finally, for the last difference, Pd-Au alloying in the first 2 ML shell, not included in the model and the small quantity of Au atoms in the shell could explain the absence of the LSPR. First, interdiffusion at Pd/Au interface is known to occur at 300 K[61] and also modifies electronic structure, the effective dielectric function and then the plasmonic response of the shell[8]. Second, for this small amount of gold on a 3 nm large Pd core, the gold shell contains around ~400 atoms and even less on smaller cores. Experimental and theoretical works have shown that localized surface plasmon arise for gold NP containing more than 300 atoms[67], in a good agreement with our findings. Finally, the onset of coalescence plays an important role in change of intensity and energy of LSPR modes. On small Pd core, a significantly thick Au shell with clear plasmonic properties can be formed and efficiently coupled to light before coalescence occurs. On large Pd core, the coalescence is rapidly reached leading to the formation of a quasi-continuous Au layer where plasmon and light can hardly couple.

If CO adsorption affects the LSPR intensity, the latter also affects the SFG response by a resonant electric field enhancement of the SFG and visible lasers that have similar energy than the LSPR (**Figure 6**). To prove it, we need to look carefully at CO band intensity at 10^{-3} mbar in **Figure 2**. The SFG intensity is raising with the shell thickness and strongly drops for 8 ML thick shell. The counting methodology of available CO adsorption sites, *i.e* Pd atoms in the shell by considering the Pd surface stoichiometry in the shell discussed before is presented in **Suppl. Materials** (**Table SM-3**, **Figure SM-7**). Only the top facet of the NP is considered, since

both SFG in *ppp* and *ssp* polarization configurations are necessary to conduct a robust orientational analysis of CO around the NP[68]. Spatial inhomogeneity of the electric field enhancement across the facet is not considered. Since the overall Pd:Au ratio is decreasing as the Au shell thickness increases, the Pd concentration at the shell surface is also decreasing. Despite a larger surface of the NP with a thicker shell, the total amount of Pd sites remains lower than for pure Pd NP. Hence, the increase of SFG response cannot be explained by the amount of Pd sites. We propose that the local electric field enhancement by the localized surface plasmon resonance as seen in simulations (**Figure 7**) is responsible for this larger SFG signal. Indeed field enhancement is spectrally broad and fully overlaps the spectral range of SFG and visible lasers leading to an enhanced SFG response as already observed[69]. An enhancement factor up to 10 is deduced by normalizing the SFG intensity by the square of the Pd sites at the shell surface (**Figure SM-7c**), as SFG is in theory proportional to the square of molecule coverage (**Equation 1**).

Impact of temperature on NP atomic structure and plasmonic response

After CO exposure of Pd/Au NPs, the surface is alloyed irreversibly and remains stable at room temperature even without CO in the chamber. In other words, after alloying the surface, CO are not involved in the stability of Pd at the shell surface and CO adsorption can reversibly be observed from low pressure to mbar pressure, on various adsorption sites on Pd (bridge: orange band, on-top on Pd dimers: violet band and > CO on-top on Pd dimers) and Au (on-top: yellow band). Two questions need to be addressed, as their answers can strongly affect NP catalytic activity *in-operando* conditions: (i) What is the depth composition profile of the shell after surface alloying? (ii) How to recover the initial core/shell phase? To answer the first question, SDRS was also employed to track the impact of Pd diffusion in the shell upon CO adsorption as well as well as the effect of CO desorption upon NP annealing. A 0.9 nm Pd core surrounded by 5 ML Au shell (7.9 Å of Au deposit) was exposed to 10^{-3} mbar of CO. This particular NP size and composition are preferred because a plasmonic response was observed without CO and 5 ML is thin enough to allow Pd diffusion to the shell surface as demonstrated above by SFG. SDRS spectra recorded at the different stage of the experiment are displayed in **Figure 8a**. It shows a slight reduction of the LSPR absorption band under CO. Finite-element-modeling of the SDRS spectrum shows a progressive damping of the LSPR as the Pd concentration increases in the last shell layer, confirming the impact of Pd diffusion to the shell surface on the plasmonic response (**Figure 8b**). It demonstrates the possibility to follow the change of plasmonic response by SDRS during, not only the growth of Au shell but also the CO exposure.

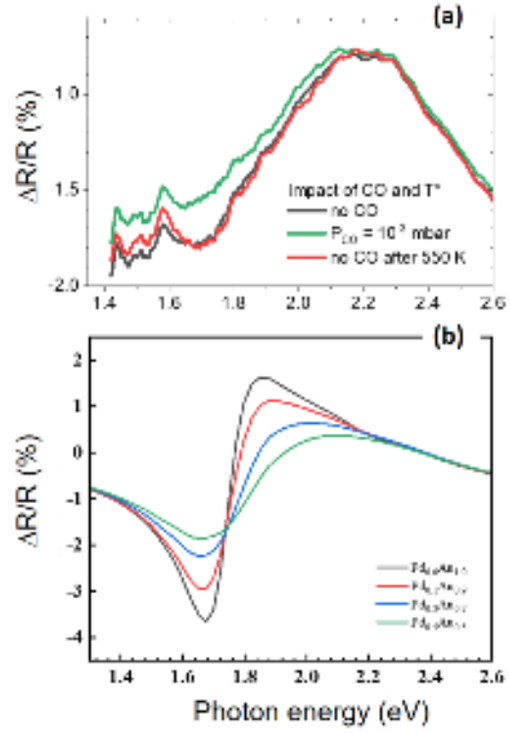

Figure 8. (a) Effect of CO adsorption and NP annealing on plasmonic response measured by SDRS on a 1.4 nm Pd surrounded by 5 ML thick Au shell. (b) Finite-element modeling of the SDRS signal for increasing Pd concentration in the last shell layer.

To answer the second question, CO was pumped from the chamber below 2.10^{-10} mbar and the sample has been annealed above 277°C (550 K) for several minutes. It allows desorbing CO from the Pd sites, leaving them free to diffuse during NP annealing and avoid any structure change of the shell surface induced by CO adsorption, desorption or reaction. SFG shows the disappearance of all CO signatures in agreement with our previous findings on Al_2O_3[28] and MgO[43]. After cooling down to 300 K and exposing again NPs to CO at low pressure ($<10^{-4}$ mbar), similar SFG spectra than for the initial core/shell state (**Figure 3**), are obtained for any shell thicknesses. After sample annealing, the LSPR is recovered in initial intensity before CO adsorption (**Figure 8**). It demonstrates that NP annealing, in addition to CO desorption, gives enough mobility to Pd (Au) atoms to migrate back towards the core (the surface, respectively) and minimizes surface energy in a good agreement with literature[37]. This leads to the recovery of initial plasmonic properties. Phase transition from a core/shell to alloyed shell NP structure accompanied with tunable plasmonic response can be cycled repetitively by adsorbing/desorbing CO and annealing the sample.

The reversible and irreversible behavior changes of the shell composition and plasmonic properties of Pd/Au core/shell NP for the different CO pressures and temperatures are summarized in **Figure 9**. A phase transition occurs above 10^{-4} mbar of CO that leads to irreversible Pd migration to the shell surface

accompanied by a reduction of the surface plasmon intensity. The Pd/Au core/shell structure and plasmonic response can be recovered by annealing NP at 550 K.

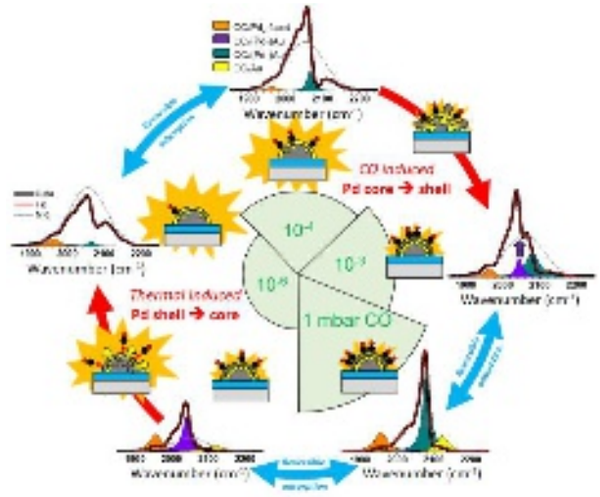

Figure 9. Core/shell to bimetallic alloy transition controlled by CO adsorption and thermal annealing. A schematic representation of the core/shell NP is given for each pressure range to illustrate phase transitions upon CO pressure and sample annealing. The reversible or irreversible transitions are indicated. Localized surface plasmon resonance intensity are represented by size of the orange spiky shape.

CONCLUSION

Pd/Au core/shell nanoparticles on alumina film have been investigated by optical spectroscopies and tunneling microscopy during growth and CO adsorption. Dipolar calculations and numerical modeling of plasmonic response of the surface support experimental findings. We have revealed how the growth of the Au shell and Pd core affects NP ordering, geometry and plasmonic properties. NP coalescence appears rapidly for shell thickness larger than 1 ML, reducing long-range order and density of NPs. Plasmonic properties are observed for shell thicker than 2 ML due to the diffusion of Pd over 2-3 ML in the Au shell. SFG vibrational spectroscopy showed that CO coverage on the shell could be tuned reversibly for pressure lower than 10^{-3} mbar as Pd concentration remains constant. Above this pressure, a new CO frequency at 2045 cm^{-1} has been observed and tentatively assigned to single CO binding on-top on Pd dimers at the surface. This band shifts to 2075±10 cm^{-1} at higher coverage when two CO adsorb on each Pd atom of the dimer. These results suggest that Pd atoms segregate in the form of dimers rather than monomers. The behavior has been observed even for thick (8 ML) gold shell. After Pd segregation, CO adsorption is not reversible from high to low pressure, unless NP are annealed above 550 K. Pd diffusion length in the shell is limited to 2-3 ML at low CO pressure and 300 K, and up to 8 ML in the mbar range. We demonstrate that the plasmonic response of the shell is

reduced by Pd diffusion to the surface under CO adsorption and can be recovered when Pd migrate back to the core after NP annealing. Finally, we evidence the impact of local field enhancement by the LSPR leading to stronger SFG response and sensitivity.

These results highlight how optical spectroscopies, in particular vibrational SFG, can bring very valuable insight about surface and bulk composition of core/shell NPs. We show that surface reactivity and plasmonic can be tuned reversibly by inducing Pd diffusion to the normally not reactive Au shell surface. This work is of great relevance for the community of heterogeneous and photo-catalysis where the control of surface composition and localized surface plasmon are required to enhance reactivity. In this respect, replacing gold by silver is a promising way to improve plasmonic response. In addition, studying the impact of CO and oxygen co-adsorption in catalytic conditions could bring additional insights on Pd segregation, phase transitions and their impact on nanoparticle reactivity.

ASSOCIATED CONTENT

Supplementary material

1. Size and composition of as grown PdAu NP
2. NP geometrical models for COMSOL modelling
3. Additional SFG spectra and analysis
4. Dipolar calculations on Pd monomers
5. SDRS spectra for 1, 2 and 3 ML Au shell thicknesses
6. Impact of surface plasmon resonance on SFG intensity

AUTHOR INFORMATION

Corresponding author: *E-mail: aimeric.ouvrard@universite-paris-saclay.fr

ORCID

Aimeric Ouvrard: 0000-0003-3652-1222

Natalia Alyabyeva: 0000-0001-5999-5821

Céline Dablemont: 0000-0003-2763-3273

Rémi Lazzari: 0000-0003-2354-1953

Fabrice Charra: 0000-0003-1228-0583

Bernard Bourguignon: 0000-0002-4171-6828

NOTES: The authors declare no competing financial interest.

ACKNOWLEDGMENTS

We thank the “Agence Nationale de la Recherche” for funding this work (LEMON project ANR-15-CE09-0007).

REFERENCES

1 M. Chen, D. Kumar, C.-W. Yi, and D. W. Goodman, “The Promotional Effect of Gold in Catalysis by Palladium-Gold”, Science Reports 310 (5746), 291-293 (2005).https://dx.doi.org/10.1126/science.1115800

2 H. C. Ham, J. A. Stephens, G. S. Hwang, J. Han, S. W. Nam, and T. H. Lim, “Role of Small Pd Ensembles in Boosting CO Oxidation in AuPd Alloys”, J. Phys. Chem. Lett. 3 (5), 566-570 (2012). https://dx.doi.org/10.1021/jz201585q

3 J.-S. Kim, H.-K. Kim, S.-H. Kim, I. Kim, T. Yu, G.-H. Han, K.-Y. Lee, J.-C. Lee, and J.-P. Ahn, “Catalytically Active Au Layers Grown on Pd Nanoparticles for Direct Synthesis of H_2O_2: Lattice Strain and Charge-Transfer Perspective Analyses”, ACS Nano 13(4), 4761-4770 (2019). https://dx.doi.org/10.1021/acsnano.9b01394

4 S. Mukherjee, F. Libisch, N. Large, O. Neumann, L. V. Brown, J. Cheng, J. B. Lassiter, E. A. Carter, P. Nordlander, and N. J. Halas, “Hot Electrons Do the Impossible: Plasmon-Induced Dissociation of H_2 on Au”, Nano Lett. 13(1), 240-247 (2013). https://dx.doi.org/10.1021/nl303940z

5 Y. Kim, D. D. Torres, and P. K. Jain, “Activation Energies of Plasmonic Catalysts”, Nano Lett. 16(5), 3399-3407 (2016). https://dx.doi.org/10.1021/acs.nanolett.6b01373

6 F. Gao, Y. Wang, and D. W. Goodman, “Reaction Kinetics and Polarization-Modulation Infrared Reflection Absorption Spectroscopy (PM-IRAS) Investigation of CO Oxidation over Supported Pd-Au Alloy Catalysts”, J. Phys. Chem. C 114(9), 4036–4043 (2010). https://dx.doi.org/10.1021/jp910896k

7 A. Hugon, L. Delannoy, J.-M. Krafft, and C. Louis, “Selective Hydrogenation of 1,3-Butadiene in the Presence of an Excess of Alkenes over Supported Bimetallic Gold-Palladium Catalysts”, J. Phys. Chem. C 114(24), 10823–10835 (2010). https://dx.doi.org/10.1021/jp100479b

8 S. Alayoglu, F. Tao, V. Altoe, C. Specht, Z. Zhu, F. Aksoy, D. R. Butcher, R. J. Renzas, Z. Liu, and G. A. Somorjai. “Surface Composition and Catalytic Evolution of Au_xPd_{1-x}(x = 0.25, 0.50 and 0.75) Nanoparticles Under CO/O_2 Reaction in Torr Pressure Regime and at 200°C”, Catal. Lett. 141, 633-640 (2011). https://dx.doi.org/10.1007/s10562-011-0565-7

9 R. Toyoshima, N. Hiramatsu, M. Yoshida, K. Amemiya, K. Mase, B. S. Mun, and H. Kondoh, “CO Adsorption on Pd−Au Alloy Surface: Reversible Adsorption Site Switching Induced by High-Pressure CO”, J. Phys. Chem. C 120(1), 416-421 (2016). https://dx.doi.org/10.1021/acs.jpcc.5b10661

10 L. Delannoy, S. Giorgio, J. G. Mattei, C. R. Henry, N. El Kolli, C. Méthivier, and C. Louis, “Surface Segregation of Pd from TiO_2-Supported AuPd Nanoalloys under CO Oxidation Conditions Observed In situ by ETEM and DRIFTS”, ChemCatChem 5(9), 2707-2716 (2013). https://dx.doi.org/10.1002/cctc.201200618

11 S. Kunz, and E. Iglesia, “Mechanistic Evidence for Sequential Displacement−Reduction Routes in the Synthesis of Pd−Au Clusters with Uniform Size and Clean Surfaces”, J. Phys. Chem. C 118(14), 7468-7479 (2014). https://dx.doi.org/10.1021/jp500537v

12 H.C. Ham, G.S. Hwang, J. Han, S.P. Yoon, S.W. Nam, and T.H. Lim, “Importance of Pd monomer pairs in enhancing the oxygen reduction reaction activity of the AuPd(100) surface: A first principles study”, Catalysis Today 263, 11-15 (2016). https://dx.doi.org/10.1016/j.cattod.2015.07.054

13 F. Gao, Y. Wang, and D.W. Goodman, “CO Oxidation over AuPd(100) from Ultrahigh Vacuum to Near-Atmospheric Pressures: The Critical Role of Contiguous Pd Atoms”, J. Am. Chem. Soc. 131(16), 5734-5735 (2009). https://dx.doi.org/10.1021/ja9008437

14 N. Chaâbane, R. Lazzari, J. Jupille, G. Renaud, and E.A. Soares, “CO-induced scavenging of supported Pt nanoclusters: a GISAXS Study”, J. Phys. Chem. C 116(44), 23362-23370 (2012). https://doi.org/10.1021/jp306496t

15 I. Laoufi, M. Saint-Lager, R. Lazzari, J. Jupille, O. Robach, S. Garaudée, G. Cabailh, P. Dolle, H. Cruguel, and A. Bailly, “Size and catalytic activity of supported gold nanoparticles: an in operando study during CO oxidation”, J. Phys. Chem. C 115(11), 4673-4679 (2011). https://doi.org/10.1021/jp1110554

16 C.-Q. Xu, M.-S. Lee, Y.-G. Wang, D.C. Cantu, J. Li, V.-A. Glezakou, and R. Rousseau, “Structural Rearrangement of Au−Pd Nanoparticles under Reaction Conditions: An ab Initio Molecular Dynamics Study”, ACS Nano 11(2), 1649-1658 (2017). https://dx.doi.org/10.1021/acsnano.6b07409

17 Y. Yanga, X. Shena, and Y.-F. Han, "Diffusion mechanisms of metal atoms in PdAu bimetallic catalyst under CO atmosphere based on ab initio molecular dynamics", Applied Surface Science 483, 991-1005 (2019). https://dx.doi.org/10.1016/j.apsusc.2019.04.036

18 H. An, H. Ha, M. Yoo, and H.Y. Kim, "Understanding the atomic-level process of CO-adsorption-driven surface segregation of Pd in $(AuPd)_{147}$ bimetallic nanoparticles", Nanoscale 9, 12077 (2017). https://dx.doi.org/10.1039/c7nr04435f

19 M. Mamatkulov, I.V. Yudanov, A.V. Bukhtiyarov, I.P. Prosvirin, V.I. Bukhtiyarov, and K.M. Neyman, "Pd Segregation on the Surface of Bimetallic PdAu Nanoparticles Induced by Low Coverage of Adsorbed CO", J. Phys. Chem. C 123(13), 8037-8046 (2019). https://dx.doi.org/10.1021/acs.jpcc.8b07402

20 H.Y. Kim, and G. Henkelman, "CO Adsorption-Driven Surface Segregation of Pd on Au/Pd Bimetallic Surfaces: Role of Defects and Effect on CO Oxidation", ACS Catal. 3(11), 2541-2546 (2013). https://dx.doi.org/10.1021/cs4006259

21 C. Garcia, V. Truttmann, I. Lopez, T. Haunold, C. Marini, C. Rameshan, E. Pittenauer, P. Kregsamer, K. Dobrezberger, M. Stöger-Pollach, N. Barrabés, and Günther Rupprechter, "Dynamics of Pd Dopant Atoms inside Au Nanoclusters during Catalytic CO Oxidation", J. Phys. Chem. C 124(43), 23626-23636 (2020). https://dx.doi.org/10.1021/acs.jpcc.0c05735

22 D. Ferrer, A. Torres-Castro, X. Gao, S. Sepulveda-Guzman, U. Ortiz-Méndez, and M. José-Yacaman, "Three-Layer Core/Shell Structure in Au−Pd Bimetallic Nanoparticles", Nanoletters 7(6), 61701-1705 (2007). https://dx.doi.org/10.1021/nl070694a

23 L. Deng, W. Hu, H. Deng, and S. Xiao, "Surface Segregation and Structural Features of Bimetallic Au-Pt Nanoparticles", J. Phys. Chem. C 114(25), 11026-11032 (2010). https://dx.doi.org/10.1021/jp100194p

24 B. Zhu, G. Thrimurthulu, L. Delannoy, C. Louis, C. Mottet, J. Creuze, B. Legrand, and H. Guesmi, "Evidence of Pd segregation and stabilization at edges of AuPd nano-clusters in the presence of CO: A combined DFT and DRIFTS study", J. of Catal. 308, 272-281 (2013). https://dx.doi.org/10.1016/j.jcat.2013.08.022

25 H.L. Abbott, A. Aumer, Y. Lei, C. Asokan, R.J. Meyer, M. Sterrer, S. Shaikhutdinov, and H.-J. Freund, "CO Adsorption on Monometallic and Bimetallic Au-Pd Nanoparticles Supported on Oxide Thin Films", J. Phys. Chem. C 114(40), 17099-17104 (2010). https://dx.doi.org/10.1021/jp1038333

26 C. Becker, A. Rosenhahn, A. Wiltner, K. von Bergmann, J. Schneider, P. Pervan, M. Milun, M. Kralj, K. Wandelt, "Al_2O_3-films on $Ni_3Al(111)$: a template for nanostructured cluster growth", New J. Phys. 4, 75 (2002). https://dx.doi.org/10.1088/1367-2630/4/1/375

27 N. Podda, M. Corva, F. Mohamed, Z. Feng, C. Dri, F. Dvorák, V. Matolin, G. Comelli, M. Peressi, and E. Vesselli, "Experimental and Theoretical Investigation of the Restructuring Process Induced by CO at Near ambient Pressure: Pt Nanoclusters on Graphene/Ir(111)", ACS Nano 11(1), 1041-1053 (2017). https://dx.doi.org/10.1021/acsnano.6b07876

28 N. Alyabyeva, A. Ouvrard, A.-M. Zakaria, and B. Bourguignon, "Probing Nanoparticle Geometry down to Subnanometer Size: The Benefits of Vibrational Spectroscopy", J. Phys. Chem. Lett. 10(3), 624-629 (2019). https://dx.doi.org/10.1021/acs.jpclett.8b03830

29 G. Sitja, A. Bailly, M.D. Santis, V. Heresanu, and C.R. Henry, "Regular Arrays of Pt Clusters on Alumina: A New Superstructure on $Al_2O_3/Ni_3Al(111)$", J. Phys. Chem. C 123(40), 24487-24494 (2019). https://dx.doi.org/10.1021/acs.jpcc.9b05109

30 G. Sitja, and C.R. Henry, "Activity of Pd_n (n = 1-5) Clusters on Alumina Film on $Ni_3Al(111)$ for CO Oxidation: A Molecular Beam Study", J. Phys. Chem. C 125(24), 13247-13253 (2021). https://pubs.acs.org/doi/10.1021/acs.jpcc.1c02060

31 G. Sitja, and C.R. Henry, "Molecular Beam Study of the CO Adsorption on a Regular Array of PdAu Clusters on Alumina", J. Phys. Chem. C 123(13), 7961-7967 (2019). https://dx.doi.org/10.1021/acs.jpcc.8b07350

32 A. Buchsbaum, M. De Santis, H.C.N. Tolentino, M. Schmid, and P. Varga, "Highly ordered Pd, Fe, and Co clusters on alumina on $Ni_3Al(111)$", Phys. Rev. B 81(11), 115420 (2010). https://dx.doi.org/10.1103/PhysRevB.81.115420

33 N.J. Divins, I. Angurell, C. Escudero, V. Pérez-Dieste, and J. Llorca, "Influence of the support on surface rearrangements of bimetallic nanoparticles in real catalysts", Science 346 (6209), 620-623 (2014). https://dx.doi.org/10.1126/science.1258106

34 S.M. Oxford, P.L. Lee, P.J. Chupas, K.W. Chapman, M.C. Kung, and H.H. Kung, "Study of Supported PtCu and PdAu Bimetallic Nanoparticles Using In-Situ X-ray Tools", J. Phys. Chem. C, 114(40), 17085-17091 (2010). https://dx.doi.org/10.1021/jp103675n

35 M. Salmeron, and R. Schlogl, "Ambient pressure photoelectron spectroscopy: A new tool for surface science and nanotechnology", Surf. Sci. Rep. 63, 169-199 (2008). https://doi.org/10.1016/j.surfrep.2008.01.001

36 B. Lim, H. Kobayashi, T. Yu, J. Wang, M.J. Kim, Z.-Y. Li, M. Rycenga, and Y. Xia, "Synthesis of Pd-Au Bimetallic Nanocrystals via Controlled Overgrowth", J. Am. Chem. Soc. 132(8), 2506-2507 (2010). https://dx.doi.org/10.1021/ja909787h

37 Z. Li, F. Gao, O. Furlong, and W.T. Tysoe, "Adsorption of carbon monoxide Au/Pd(100) alloys in ultrahigh vacuum: Identification of adsorption sites", Surface Science 604, 136-143 (2010). https://dx.doi.org/10.1016/j.susc.2009.10.031

38 M. Melchionna, and P. Fornasiero, "Updates on the Roadmap for Photocatalysis", ACS Catal. 10(10), 5493-5501 (2020). https://doi.org/10.1021/acscatal.0c01204

39 N. Alyabyeva, A. Ouvrard, A.-M. Zakaria, F. Charra, and B. Bourguignon, "Transition from Disordered to Long-Range Ordered Nanoparticles on $Al_2O_3/Ni_3Al(111)$", Appl. Surf. Sci. 444, 423-429 (2018). https://dx.doi.org/10.1016/j.apsusc.2018.03.025

40 I. Horcas, R. Fernández, J.M. Gómez-Rodríguez, J. Colchero, J. Gómez-Herrero, and A.M. Baro, "WSXM: A Software for Scanning Probe Microscopy and a Tool for Nanotechnology". Rev. Sci. Instrum. 78, 013705 (2007). https://dx.doi.org/10.1063/1.2432410

41 Y.R. Shen, "Surface properties probed by second-harmonic and sum-frequency generation", Nature 337, 519-525 (1989). https://doi.org/10.1038/337519a0

42 R.W. Boyd, "Nonlinear Optics", Academic Press, Harcourt Brace Jovanovich: 1992.

43 A. Ouvrard, A. Ghalgaoui, C. Michel, C. Barth, J. Wang, S. Carrez, W. Zheng, C.R. Henry, and B. Bourguignon, "CO Chemisorption on Ultrathin MgO-Supported Palladium Nanoparticles", J. Phys. Chem. C 121(10), 5551−5564 (2017). https://dx.doi.org/10.1021/acs.jpcc.6b10595

44 A. Ghalgaoui, A. Ouvrard, J. Wang, S. Carrez, W. Zheng, and B. Bourguignon, "Electron to Adsorbate Energy Transfer in Nanoparticles: Adsorption Site, Size, and Support Matter", J. Phys. Chem. Lett. 8(12), 2666-2671 (2017). https://dx.doi.org/10.1021/acs.jpclett.7b00698

45 A. Ghalgaoui, R. Horchani, A. Ouvrard, J. Wang, S. Carrez, and B. Bourguignon, "Identification of Active Sites in Oxidation Reaction from Real-Time Probing of Adsorbate Motion over Pd Nanoparticles", J. Phys. Chem. Lett. 9(18), 5202-5206 (2018). https://dx.doi.org/10.1021/acs.jpclett.8b02215

46 M. Marsault, G. Sitja, and C.R. Henry, "Regular Arrays of Pd and PdAu Clusters on Ultrathin Alumina Films For Reactivity Studies", Phys. Chem. Chem. Phys. 16, 26458-26466 (2014). https://dx.doi.org/10.1039/C4CP02200A

47 J. Wang, H. Dubost, A. Ghalgaoui, W. Zheng, S. Carrez, A. Ouvrard, and B. Bourguignon, "Effect of Visible Pulse Shaping on the Accuracy of Relative Intensity Measurements in BBSFG Vibrational Spectroscopy", Surf. Sci. 626, 26-39 (2014). https://dx.doi.org/10.1016/j.susc.2014.03.017

48 R. Lazzari, and J. Jupille, "Growth Kinetics and Size-Dependent Wetting of Ag/α-Al_2O_3(0001) Nanoparticles Studied via the Plasmonic Response". Nanotechnology 23(13), 135707 (2012). https://dx.doi.org/10.1088/0957-4484/23/13/135707

49 R. Lazzari, J. Jupille, R. Cavallotti, and I. Simonsen, "Model-Free Unraveling of Supported Nanoparticles Plasmon Resonance Modes", J. Phys. Chem. C 118(13), 7032-7048 (2014). https://dx.doi.org/10.1021/jp500675h

50 N. Alyabyeva, A. Ouvrard, R. Lazzari, and B. Bourguignon, "Ordered Hybrid Assembly of Palladium Nanoparticles and Perylene Molecules on an Alumina Template", J. Phys. Chem. C 123(31), 19175-19182 (2019). https://dx.doi.org/10.1021/acs.jpcc.9b04147

51 G.D. Mahan, and A.A. Lucas, "Collective Vibrational Modes of Adsorbed CO", J. Chem. Phys. 68(4), 1344-1348 (1978). https://doi.org/10.1063/1.435952

52 B.N.J. Persson, and R. Ryberg, "Vibrational Interaction Between Molecules Adsorbed on a Metal Surface: The Dipole-Dipole Interaction", Phys. Rev. B: Condens. Matter Mater. Phys. 24(12), 6954-6970 (1981). https://doi.org/10.1103/PhysRevB.24.6954

53 A. Ouvrard, J. Wang, A. Ghalgaoui, S. Nave, S. Carrez, W. Zheng, H. Dubost, and B. Bourguignon, "CO Adsorption on Pd(100) Revisited by Sum Frequency Generation: Evidence for Two Adsorption Sites in the Compression Stage", J. Phys. Chem. C 118(34), 19688-19700 (2014). https://dx.doi.org/10.1021/jp500912p

54 M. Cho, C. Hess, and M. Bonn, "Lateral Interactions Between Adsorbed Molecules: Investigations of CO on Ru(001) Using Nonlinear Surface Vibrational Spectroscopies", Phys. Rev. B: Condens. Matter Mater. Phys. 65(20), 205423 (2002). https://doi.org/10.1103/PhysRevB.65.205423

55 B.N.J. Persson, and F.M. Hoffmann, "Vibrational Phase Relaxation at Surfaces: The Role of Lateral Interaction", J. of Electron. Spectroscopy and Related Phenomena 45, 215-225 (1987). https://doi.org/10.1016/0368-2048(87)80070-1

56 H. Kato, H. Okuyama, S. Ichihara, M. Kawai, and J. Yoshinobu, "Lateral Interactions of CO in the (2 × 1)p2mg Structure on Pd(110): Force Constants Between Tilted CO Molecules", J. Chem. Phys. 112(4), 1925-1936 (2000). https://doi.org/10.1063/1.480771

57 A. Ortega, F.M. Hoffman, and A.M. Bradshaw, "The Adsorption of CO on Pd(100) Studied by IR Reflection Absorption Spectroscopy", Surf. Sci. 119, 79-94 (1982). https://doi.org/10.1016/0039-6028(82)90189-3

58 M. Schmid, G. Kresse, A. Buchsbaum, E. Napetschnig, S. Gritschneder, M. Reichling, and P. Varga, "Nanotemplate with Holes: Ultrathin Alumina on $Ni_3Al(111)$", Phys. Rev. Lett. 99(19), 196104 (2007). https://dx.doi.org/10.1103/PhysRevLett.99.196104

59 J.M. Rahm, C. Tiburski, T.P. Rossi, F.A. Ardy Nugroho, S. Nilsson, C. Langhammer, and P. Erhart, "A Library of Late Transition Metal Alloy Dielectric Functions for Nanophotonic Applications", Adv. Funct. Mater. 30(35), 2002122 (2020). https://dx.doi.org/10.1002/adfm.202002122

60 A. Bailly, G. Sitja, M.-C. Saint-Lager, S. Le Moal, F. Leroy, M. De santis, C.R. Henry, and O. Robach, "Influence of palladium on the ordering, the final size and composition of Pd-Au nanoparticle arrays", J. Phys. Chem. C 121(46), 25864-25874 (2017). https://dx.doi.org/10.1021/acs.jpcc.7b08254

61 F. Gao, Y. Wang, and W.D. Goodman, "CO Oxidation over AuPd(100) from Ultrahigh Vacuum to Near-Atmospheric Pressures: CO Adsorption-Induced Surface Segregation and Reaction Kinetics", J. Phys. Chem. C 113(33), 14993-15000 (2009). https://dx.doi.org/10.1021/jp9053132

62 W.R. Tyson, and W.A. Miller, "Surface free energies of solid metals: Estimation from liquid surface tension measurements", Surf. Sci. 62(1), 267-276 (1977). https://doi.org/10.1016/0039-6028(77)90442-3

63 M. Morkel, H. Unterhalt, M. Salmeron, G. Rupprechter, and H.-J. Freund, "SFG spectroscopy from 10^{-8} to 1000 mbar: less-ordered CO structures and coadsorption on Pd(111)", Surf. Sci. 532-535, 103-107 (2003). https://doi.org/10.1016/S0039-6028(03)00197-3

64 M. Morkel, G. Rupprechter, and H.-J. Freund, "Finite size effects on supported Pd nanoparticles: Interaction of hydrogen with CO and C_2H_4", Surf. Sci. Lett. 588(1-3), L209-L219 (2005). https://doi.org/10.1016/j.susc.2005.05.037

65 R. Lässer and N. V. Smith, "Interband optical transitions in gold in the photon energy range 2-25 eV", Solid State Communications 37(6), 507-509 (1981). https://doi.org/10.1016/0038-1098(81)90488-9

66 H. Ditlbacher, J. R. Krenn, G. Schider, A. Leitner, and F. R. Aussenegg, "Two-dimensional optics with surface plasmon polaritons", Appl. Phys. Lett. 81(10), 1762-1764 (2002). https://doi.org/10.1063/1.1506018

67 S. Malola, L. Lehtovaara, J. Enkovaara, and H. Häkkinen, "Birth of the Localized Surface Plasmon Resonance in Monolayer-Protected Gold Nanoclusters", ACS Nano 7(11), 10263-10270 (2013). https://dx.doi.org/10.1021/nn4046634

68 V. Pramhaas, H. Unterhalt, H.-J. Freund, and G. Rupprechter, "Polarization-Dependent Sum-Frequency-Generation Spectroscopy for In Situ Tracking of Nanoparticle Morphology", Angew. Chem. Int. Ed. 62(19), e202300230 (2023). https://doi.org/10.1002/anie.202300230

69 C. Humbert, O. Pluchery, E. Lacaze, B. Busson, and A. Tadjeddine, "Two-Colour Sum-Frequency Generation Spectroscopy Coupled to Plasmonics with the CLIO Free Electron Laser", Photonics 9(22), 55 (2022). https://doi.org/10.3390/photonics9020055